

**DETECTION OF STREAMFLOW CHANGE TO PREVENT RESIDENTS FROM POTENTIAL
DISASTERS**

*J. -H. Chen, M. -C. Su, and J. Chen
National Central University
300 Jhongda
Jhongli, Taoyuan 32001, Taiwan.
(*Corresponding author: jhchen@ncu.edu.tw)

DETECTION OF STREAMFLOW CHANGE TO PREVENT RESIDENTS FROM POTENTIAL DISASTERS

ABSTRACT

Remote sensing technologies have been applied to numerous fields and already benefited those in improving efficiency and recognition accuracy. Change of streamflow can be devastating to residents living along riversides. Still it is difficult to detect such deathly change in large area scale by traditional field surveys. The research aims at provision of detecting streamflow change using a mathematic method based on remote sensing technologies. The scope is on remote sensing stream images taken during the invasion by Typhoon Morakot, bringing one of the major catastrophes to Taiwan. An algorithm was adopted to deal with streamflow recognition on RGB images. The algorithm is capable of yielding change measured by meters and illustrates how main streams shift. An practical example for the Baolai area surrounded by Laonong stream shows that the streamflow moved 88 meters (36 pixels) toward the downtown area during the invasion by Typhoon Morakot. In addition, the results highlight all dangerous zones (scouring zones) for residents to prevent further potential damage.

KEYWORDS

Remote sensing, RGB image, Disaster prevention, Automatic detection, Pattern recognition.

INTRODUCTION

The Taiwan Island comprising approximately 50% mountain area of the total is located in the Eastern Pacific region. There are 258 mountains exceeding in the altitude of 3,000 meters in the island whose area is only 36,190 square kilometers. Moreover, the annual precipitation reaches 2,515 millimeters. The amount in the mountain areas is usually double or even more. This can be seen from the maximum annual precipitation of 9,513 millimeters that occurred in the northeastern mountain area, and the maximum daily precipitation of 1,403 millimeters that fell in the southern mountain area (Central Weather Bureau, 2013). The unique climate and terrain shape rivers and streams severely. Most of them have a principal common characteristic of short with strong scouring capability that causes their courses being changed frequently. Residents live by or near rivers and streams potentially suffer economic loss or even threat to their lives. For example, Typhoon Morakot dumped record-breaking amount of precipitation in Taiwan during the invasion in 2008, causing catastrophic economic losses and claiming 699 lives. Among the losses, 491 lives lost directly due to complete devastation of a village by a stream that changed its course. As a result, it is an urgent need to detect changes of river courses in an effective way so as to protect residents living among rivers from potential natural disasters.

Field measurement is a basic and traditional approach to record change of surroundings. Yet, field survey processes are typically perplexed at time-consuming and manpower shortage. Solutions associated with easy access and manpower efficiency drive practitioners to develop feasible alternatives. Numerous types of images have been utilized to recognize changes of terrain. These include ultrasound spectroscopy, laser imagery, remote sensing imagery, synthetic aperture radar imagery, and thermal imaging (Muller *et al.* 2006, Olsen *et al.* 2010, Su *et al.* 2011, Brunner *et al.* 2010, Newaz and Chen 2005). The use of remote sensing imagery to large scale recognition is common due to image accessibility and relatively high accuracy. Related work has shown that remote sensing is an effective technique for recognizing damaged areas (Tsutsui *et al.* 2007, Lee *et al.* 2008). Vegetation change can be measured using remote sensing analysis. Estimation of crop damage traditionally depends on the technique of field observations, which is a time-consuming task, but it has proven rapid accessible and feasible to exploit remote sensing imagery for this purpose (Silleos *et al.* 2002). A related study has been carried out to identify damage to cotton crops through the use of remote sensing images, also indicating that multispectral imaging is a viable tool (Huang *et al.* 2010). Mapping based on the analysis of remote sensing images has been utilized by rescuers (Stramondo *et al.* 2006). For example, the mapping of earthquake damage assessment has been proposed as a means of assisting rescuers in developing rescue plans (Cheema 2007). Remote sensing imagery has been integrated with GIS techniques to facilitate damage assessment after tsunami invasion in southern Asia, 2004 (Kurmar *et al.* 2007). Other studies have pointed out the benefits of using remote sensing imagery to estimate the impact of tsunamis (Liu *et al.* 2007, Bovolo *et al.* 2007, Dharanirajan *et al.* 2007,

Sirikulchayanon *et al.* 2008, Kerr *et al.* 2009). A rapid recognition approach for built-up structures has already been developed with applications elaborated in succeeding studies (Voigt *et al.* 2011). Forest management is another field that frequently makes use of remote sensing techniques to recognition problems, such as for timber resource investigation, detection of forest fires, monitoring of carbon emissions and forest damage, and so on (Ekstrand 1996, Isaev *et al.* 2002, Lee *et al.* 2008, Stone *et al.* 2008). Investigation shows the high accuracy of image-based assessment compared to field inventory estimates. It is suggested that pre-disturbance field inventory data should not require for satellite image-based assessment. The use of remote sensing image methods will no doubt save efforts while providing high accuracy for large-scale damage assessment. The research objective is to determine tendency change for river streamflow based on recognition using remote sensing imagery. The imagery in the study is based on (1) the acquisition of remote sensing images from a single satellite (FORMOSAT-2), (2) the use of remote sensing RGB images that have already been calibrated and fine-tuned, and (3) manual recognition by experts and field observations that are involved as the final validation for pattern classification. Additionally, with the aspects of better recognition and social benefit, the imagery collection considers a river that experienced extreme volume of current and that flew by village(s) with relatively high density of population.

RECOGNITION METHODS FOR REMOTE SENSING IMAGES

Various techniques capable of handling different demands for image recognition have already been developed. Over two decades ago, scientists started to track contamination in forests using remote sensing techniques (Airola 1990). In 1999, Bernstein and Di Gesù developed an object recognition system to extract shape information from remote sensing images. Melgani (2002) developed an unsupervised change-detection method that achieved a better estimate of the optimal threshold value. Later a clustering technique was adopted to detect deterioration of structures for damage assessment. The study performed a comparison of four algorithms employed to detect forest change due to hurricane invasion: univariate image differencing (UID), selective principal component analysis (PCA), change vector analysis (CVA), and post-classification comparison (PCC) (Kabir *et al.* 2009). The last one, along with the composite image, yielded the best results, but all four algorithms were still subject to some restrictions. A probabilistic classification framework was developed to provide posterior probabilities for urban regions. The approach was able to classify damage levels that deterministic approaches could not solve (Chen and Hutchinson 2010). However, remote sensing techniques have rarely been adopted to measure changes in rivers, although some, such as the k nearest neighbor (KNN), objective-oriented supervised classification, raster-based classification (Johansen *et al.* 2008, Pavelsky *et al.* 2008) techniques, can be found. Measuring change of river courses remains barely untouched.

REMOTE SENSING IMAGES AND DETECTION MODEL

Remote sensing images used for the study are acquired based on the geometry-calibrated imagery from the FORMOSAT-2 satellite. The images have high resolution with the following characteristics: (1) multispectral resolution of 8m, (2) RGB wavelength from 0.45 to 0.69 μm , and (3) image swath of 24km with a limb view angle $\pm 45^\circ$. Geometric calibration of the images is carried out to eliminate spatial errors as precision ground control points and digital terrain model are available. To eliminate errors for targeted images, we apply linear deformation as an affine transformation plus manually digitized image control points (Liou *et al.* 2010). As limited to the research scope, the preselected FORMOSAT-2 satellite image is show in Figure 1. One can see that there were almost no landslides upstream before the flooding. It is clear that the record-high amount of precipitation did cause significant changes in the river bed. The residential areas were lessened due to the course change by the river. The proposed method is first to utilize FORMOSAT-2 images, belonging to the RGB image type. Starting with the threshold settings of RGB pixels from 0 to 255, we determine the settings for forest, for instance, by the following expression:

$$I'(x,y) = \begin{cases} I(x,y), & \text{if } 140 \leq B_{xy} \leq 255 \text{ and } 50 \leq R_{xy} \leq 255 \\ 0, & \text{else} \end{cases}, \quad (1)$$

where $I'(x,y)$ is the labeled RGB value of the pixel I at (x,y) coordination; $I(x,y)$ is the original RGB value for the pixel I ; and B_{xy} and R_{xy} represent the blue and red values of the pixel I . Comparing these two images,

we are able to obtain an assessment of the damaged forest area. Assuming that P_{ij} represents the pixel at (i, j) , the illustration in Figure 2 demonstrates how the comparison works.



Figure 1 – Baolai-2 Bridge and its surroundings before and after Typhoon Morakot struck

P_{i1j1} (25)	P_{i2j1} (30)	P_{i3j1} (31)
P_{i1j2} (13)	P_{center} (65)	P_{i3j2} (65)
P_{i1j3} (3)	P_{i2j3} (89)	P_{i3j3} (68)

Before disaster

P_{i1j1} (20)	P_{i2j1} (35)	P_{i3j1} (30)
P_{i1j2} (13)	P_{center} (15)	P_{i3j2} (15)
P_{i1j3} (3)	P_{i2j3} (66)	P_{i3j3} (72)

After disaster

P_{i1j1} (5)	P_{i2j1} (-5)	P_{i3j1} (1)
P_{i1j2} (0)	P_{center} (50)	P_{i3j2} (50)
P_{i1j3} (0)	P_{i2j3} (23)	P_{i3j3} (-4)

Difference

Figure 2 – Comparison of before and after disaster images

Similarly the built-up area can be also estimated following this process. For river image recognition, there are two steps, dilation and erosion, to compute changes in the rivers. The dilation step finds any pixel in the river with its $I' = 0$ and then identifies its neighboring I' values in a smallest area (3 by 3). Once any neighbor with $I' \neq 0$ is spotted, the proposed model resets its value to 0. After a certain number of pre-determined iterations determined or no more pixel $I' \neq 0$ found, the dilation stops, and the next step of erosion kicks in. The erosion step is similar to a reversed process of the dilation step designed to restore the original river pixels without noise. In this step, the proposed model seeks those pixels being “dilated” in the last step. Finding a “dilated” pixel with $I' \neq 0$, the proposed model sets all $I' = 1$ when spotting any $I' = 0$ in the smallest neighbor area. This step is repeated until the pre-specified number of iterations is reached or no more $I' = 0$ pixels are found. Now, the river width can be calculated. The proposed model also measures river changes. Heavy precipitation may trigger landslides or flooding that presents similar images, which causes difficulty for recognition. The additional function of skeletonization provided by the proposal model outlines the main river course, detects new stream courses, and differentiates flooding or landslide areas. These tasks can be done through the determination of the river’s “skeleton”. Assuming that in an M by N neighboring pixel area, we define $N(P) = \sum_{i=1; j=1}^{i=M; j=N} p_{ij} (1)$ and $S(P) = \sum_{i=1; j=1}^{i=M; j=N} p_{ij} (0)$, as illustrated in Figure 3. To facilitate computation, M and N are usually set to be a smallest neighbor area (3 by 3). All pixels in the area are removed if satisfying

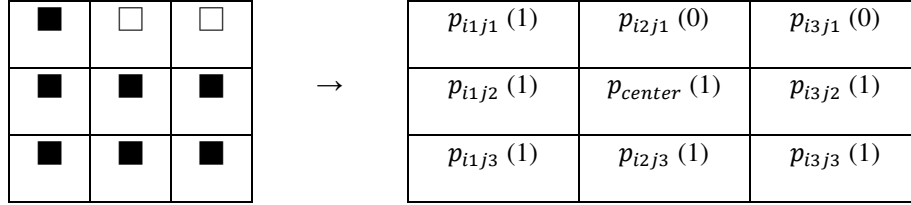


Figure 3 – Illustration for river skeletonization

$$if \left(\begin{matrix} 2 \leq N(P) \leq 6; S(P) = 1; P_{i2j1} \cdot P_{i3j2} \cdot P_{i2j3} = 0; P_{i3j2} \cdot P_{i2j3} \cdot P_{i1j2} = 0 \\ 2 \leq N(P) \leq 6; S(P) = 1; P_{i2j1} \cdot P_{i3j2} \cdot P_{i1j2} = 0; P_{i2j1} \cdot P_{i2j3} \cdot P_{i1j2} = 0 \end{matrix} \right) \quad (2)$$

Then all pixels are removed.

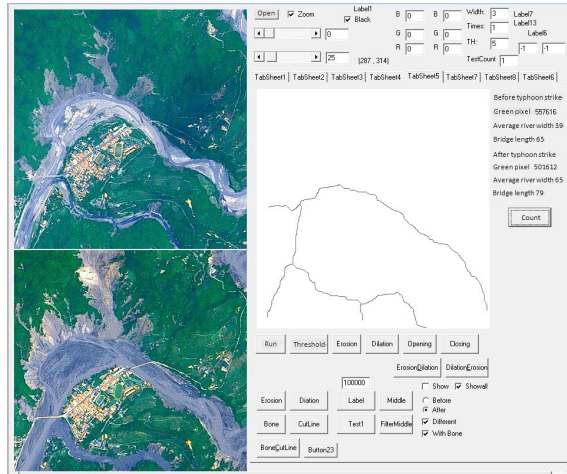


Figure 4 – River course and results

However, no pixel is removed when satisfying $N(P) = 0$, $N(P) = 1$, $N(P) > 6$, or $S(P) = 0$, where the pixel represents the edge point. The proposed model is complete. Figure 4 presents a demonstration of the model interface using the C++ language. Applying the model to Figure 1 and then overlapping two courses, we obtain the result showing in Figure 5. The evaluation to measure accuracy is conducted based on manual check by experts. Figure 6 shows the evaluation results by experts and also a comparison of changes in the river width. Both manual and model recognition measures 88 meter erosion to the densest residential area. The results are relatively accurate based on the resolution of the images (± 8 meters). A measurement of 88 meter erosion to the densest residential area, which makes up almost $\frac{1}{4}$ of the area in width, represents significant threats to residents.

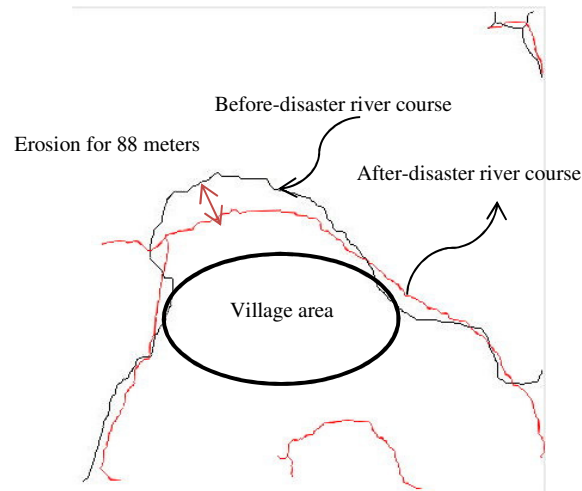


Figure 5 – Results for course change



Figure 6 – Comparison of changes in the river

CONCLUSION

The research intends to detect change of river courses caused by strong streamflow. The proposed model is designed to provide quick and precise measurement of changes in river courses, river width, and scouring sites. By outlining the river skeleton and revealing the river courses, it is found that the broken segment is located exactly at one of the scoured sides of the river. The accuracy is also demonstrated in the example measuring the shore-to-shore river width. The extra contributions can be summarized as presenting a novel technique that effectively allows large-scale assessment with high accuracy and notation for follow-up monitoring. Further utilizing the results from this research, succeeding studies could gain more valuable information in practice. Examples can be expected for a warning system or a prediction model that may be accordingly created to prevent loss of life and lessen impact on economic activities. The scope or feasibility of the proposed model could be extended to other research fields so as to benefit human beings.

REFERENCES

Airola, T. M., (1990). Monitoring the impact of arsenic contamination on forest vegetation in New Jersey using remote sensing techniques. *Journal of imaging technology*, 16, 120-123.

- Bovolo, F., & Bruzzone, L., (2007). A split-based approach to unsupervised change detection in large-size multitemporal images: application to tsunami-damage assessment. *IEEE Transactions on Geoscience and Remote Sensing*, 45, 1658-1669.
- Brunner, D., Lemoine, G., & Bruzzone, L., (2010). Earthquake damage assessment of buildings using VHR optical and SAR imagery. *IEEE Transactions on Geoscience and Remote Sensing*, 48, 2403-2420.
- Central Weather Bureau (2013). *Historical Data*. Retrieved from http://www.cwb.gov.tw/V7/index_home.htm
- Cheema, U., (2007). Expert systems for earthquake damage assessment. *IEEE Aerospace and Electronic Systems Magazine*, 22, 6-10.
- Chen, Z. & Hutchinson, T. C., (2010). Probabilistic urban structural damage classification using bitemporal satellite images. *Earthquake Spectra*, 26, 87-109.
- Dharanirajan, K., Kasinatha P. P., Gurugnanam, B., Narayanan, R. M., & Ramachandran, S., (2007). An integrated study for the assessment of tsunami impacts: A case study of South Andaman Island, India using remote sensing and GIS. *Coastal Engineering Journal*, 49, 229-266.
- Ekstrand, S., (1996). Landsat TM-based forest damage assessment: Correction for topographic effects. *Photogrammetric Engineering and Remote Sensing*, 62, 151.
- Huang, Y., Thomson, S. J., Ortiz, B.V., Reddy, K.N., Ding, W., Zablotowicz, R.M., & Bright, J. R., (2010). Airborne remote sensing assessment of the damage to cotton caused by spray drift from aerially applied glyphosate through spray deposition measurements. *Biosystems Engineering*, 107, 212-220.
- Isaev, A. S., Korovin, G.N., Bartalev, S. A., Ershov, D. V., Janetos, A., Kasischke, E. S., Shugart, H. H., French, N. H. F., Orlick, B. E., & Murphy, T.L., (2002). Using remote sensing to assess Russian forest fire carbon emissions. *Climatic Change*, 55, 235-249.
- Johansen, K., Phinn, S., Lowry, J., & Douglas, M., (2008). Quantifying indicators of riparian condition in Australian tropical savannas: Integrating high spatial resolution imagery and field survey data. *International Journal of Remote Sensing*, 29, 7003-7028.
- Kabir, S., Rivard, P., He, D. -C., & Thivierge, P., (2009). Damage assessment for concrete structure using image processing techniques on acoustic borehole imagery. *Construction and Building Materials*, 23, 3166-3174.
- Kerr, A. M., Baird, A. H., Bhalla, R. S., & Srinivas, V., (2009). Reply to 'Using remote sensing to assess the protective role of coastal woody vegetation against tsunami waves'. *International Journal of Remote Sensing*, 30, 3817-3820.
- Kumar, A., Chingkhei, R. K., & Dolendro, T., (2007). Tsunami damage assessment: A case study in Car Nicobar Island, India. *International Journal of Remote Sensing*, 28, 13-14, 2937-2959.
- Lee, M. -F., Lin, T. -C., Vadeboncoeur, M. A., & Hwong, J. -L., (2008). Remote sensing assessment of forest damage in relation to the 1996 strong typhoon Herb at Lienhuachi Experimental Forest, Taiwan. *Forest Ecology and Management*, 255, 3297-3306.

- Liou, Y. A., Kar, S. K., & Chang, L. Y., (2010). Use of high-resolution FORMASAT-2 satellite images for post-earthquake disaster assessment: A student following 12 May 2008 Wenchuan earthquake. *International Journal of Remote Sensing*, 31, 3355-3368.
- Liu, C.-C., Liu, J.-G., Lin, C.-W., Wu, A.-M., Liu, S.-H., & Shieh, C.-L., (2007). Image processing of FORMOSAT-2 data for monitoring the South Asia tsunami. *International Journal of Remote Sensing*, 28, 3093-3111.
- Melgani, F., Moser, G., & Serpico, S. B., 2002. Unsupervised change-detection methods for remote-sensing images. *Optical Engineering*, 41, 3288-3297.
- Muller, M., Tencate, J.A.; Darling, T.W., Sutin, A., Guyer, R.A., Talmant, M., Laugier, P., & Johnson, P.A., (2006). Bone micro-damage assessment using non-linear resonant ultrasound spectroscopy (NRUS) techniques: A feasibility study. *Ultrasonics*, 44, 245-249.
- Newaz, G. & Chen, X., 2005. Progressive damage assessment in thermal barrier coatings using thermal wave imaging technique. *Surface and Coatings Technology*, 190, 7-14.
- Olsen, M. J., Kuester, F., Chang, B. J., & Hutchinson, T. C., (2010). Terrestrial laser scanning-based structural damage assessment. *Journal of Computing in Civil Engineering*, 24, 264-272.
- Pavelsky, T. M. & Smith, L. C., (2008). RivWidth: A software tool for the calculation of river widths from remotely sensed imagery. *IEEE Geoscience and Remote Sensing Letters*, 5, 70-73.
- Silleos, N., Perakis, K., & Petsanis, G., (2002). Assessment of crop damage using space remote sensing and GIS. *International Journal of Remote Sensing*, 23, 417-427.
- Sirikulchayanon, P., Sun, W., & Oyana, T., (2008). Assessing the impact of the 2004 tsunami on mangroves using remote sensing and GIS techniques. *International Journal of Remote Sensing*, 29, 3553-3576.
- Stone, C., Turner, R., & Verbesselt, J., (2008). Integrating plantation health surveillance and wood resource inventory systems using remote sensing. *Australian Forestry*, 71, 245-253.
- Stramondo, S., Bignami, C., Chini, M., Pierdicca, N., & Tertulliani, A., (2006). Satellite radar and optical remote sensing for earthquake damage detection: Results from different case studies. *International Journal of Remote Sensing*, 27, 4433-4447.
- Su, M. -C., Huang, D. -Y., Chen, J. -H., Lu, W. -Z, Tsai, L. -C., & Lin, J. -Z., (2011). Mapping multi-spectral remote sensing images using rule extraction approach. *Expert Systems with Applications*, 38, 12917-12922.
- Tsutsui, K., Rokugawa, S., Nakagawa, H., Miyazaki, S., Cheng, C. -T., Shiraishi, T., & Yang, S. -D., (2007). Detection and volume estimation of large-scale landslides based on elevation-change analysis using DEMs extracted from high-resolution satellite stereo imagery. *IEEE Transactions on Geoscience and Remote Sensing*, 45, 1681-1696.
- Voigt, S., Schneiderhan, T., Twele, A., Gähler, M., Stein, E., & Mehl, H., (2010). Rapid damage assessment and situation mapping: Learning from the 2010 Haiti earthquake. *Photogrammetric Engineering and Remote Sensing*, 77, 923-931.